Quantum dynamics of a 4π kink in Josephson junction parallel arrays with large kinetic inductance

S. S. Seidov [1] and M. V. Fistul [2]

[1] *National University of Science and Technology "MISIS," Moscow 119049, Russia*
[2] *Theoretische Physik III, Ruhr-Universität Bochum, Bochum 44801, Germany*

(Received 21 June 2022; revised 11 November 2022; accepted 30 November 2022; published 9 December 2022)

We present a theoretical study of the quantum dynamics of *two* magnetic fluxons trapped in Josephson junction parallel arrays (JJPAs) with large kinetic inductances. The Josephson phase distribution of two trapped magnetic fluxons satisfies a topological constraint, i.e., the total variation of Josephson phases along a JJPA is 4π. In such JJPAs the characteristic length of the Josephson phase distribution ("the size" of magnetic fluxon) is drastically reduced to be less than a single cell size. Two extreme dynamic patterns will be distinguished: two weakly interacting and two merged magnetic fluxons, i.e., a 4π kink. Taking into account the repulsive interaction between two magnetic fluxons located in the same or adjacent cells, we obtain the energy band spectrum $E_{4\pi}(p)$ for a quantum 4π kink. The coherent quantum dynamics of 4π kinks demonstrates the quantum beats with the frequency and amplitude strongly deviating from those observed for two independent magnetic fluxons. In the presence of applied dc and ac bias currents of frequency f a weakly incoherent quantum dynamics of a 4π kink results in the Bloch oscillations and the seminal current steps with values $I_{4\pi}^{(n)} = enf$ which are two times less than those for two independent magnetic fluxons.

DOI: 10.1103/PhysRevB.106.224507

I. INTRODUCTION

Magnetic fluxons (MFs) are topological solitons [1–4] studied intensively in various low-dimensional superconducting systems, e.g., in Josephson junction parallel arrays (JJPAs) [5–8]. Each MF is a vortex of superconducting current carrying one magnetic flux quantum, Φ_0. The JJPAs composed of a large number of superconducting cells with embedded Josephson junctions, have provided a well established experimental platform for studying the MFs dynamics. A variety of fascinating physical phenomena in the classical nonlinear dynamics of MFs have been observed experimentally, e.g., dc/ac current induced resonances [5], the relativistic dynamics of MF [6], bunching of MFs [9], the Cherenkov radiation of plasma modes by moving MF [10], ac current induced dynamic metastable states [11], and the dynamics of MFs in a specially prepared ratchet potential [12]. The MF itself is a 2π kink in the spatial distribution of Josephson phases [5,6]. The effective methods have been elaborated to trap, manipulate, and to measure MFs in JJPAs.

Even more complex macroscopic objects, e.g., breathers, i.e., (anti)MF-MF pairs, observed in long Josephson junctions [6,7], discrete breathers trapped in Josephson junction ladders [13,14], or high-order kink states in JJPAs [9,15–18], have been theoretically and experimentally studied. The latter have been predicted a long time ago [15,16] and, in spite of the repulsion of two MFs approaching each other, moving 4π *kinks* have been experimentally observed in Ref. [18]. The fingerprint of the 4π kink nonlinear classical dynamics is a specific branch of the current-voltage characteristics (I-V curve) substantially deviating from the one related to the motion of two independent MFs. The effective numerical procedures have been developed in order to quantitatively analyze the classical dynamics of MFs and high-order kinks in JJPAs governed by a large set of coupled nonlinear differential equations with topological constraints [6,7].

A new twist in this field, namely, a study of the *quantum* dynamics of macroscopic topological objects, has attracted great interest. Initial studies have demonstrated a large number of incoherent quantum phenomena such as the macroscopic quantum tunneling of a bunch of MFs in two-dimensional Josephson junction arrays [19,20], the macroscopic quantum tunneling and energy level quantization of a single MF [21–25] in specially prepared potential, and the quantum dissociation of a vortex-antivortex pair [26] in long annular Josephson junctions. It was realized that the main obstacle on the way to observe the *coherent* quantum-mechanical effects in the dynamics of MFs is a large spatial extent (the MFs "size") of a 2π kink greatly exceeding the size of a single cell. The quantum dynamics of various excitations in such JJPAs have been successfully described by the seminal sine-Gordon equation [27–29]. However, the sine-Gordon equation being an integrable one, does not allow the formation of 4π kinks and an intrinsic Peierls-Nabarro potential, and various nontopological macroscopic objects, e.g., the plasma oscillations or vortex-antivortex pairs, can easily be excited leading to an additional dissipation and decoherence in the dynamics of MFs.

In order to drastically decrease the MFs size one needs to replace low geometrical inductances by large kinetic ones. Implementation of large kinetic inductances in JJPAs or long Josephson junctions can be provided by two effective methods: an embedding of series arrays of large Josephson junctions in each cell of JJPAs [30,31], or using disordered superconducting materials [32–35].

The coherent quantum dynamics of a single MF trapped in a JJPA with large kinetic inductances have been theoretically studied in [31,36,37]. In such JJAs the Josephson phases strongly vary from one cell to adjacent cells, and therefore, the discrete sine-Gordon equation in an almost anticontinuous limit [4,36,38] can be used to describe the quantum dynamics of MFs. Such coherent quantum-mechanical effects as the quantum beats of a single MF in JJAs composed of a few cells [31], the MF energy band [36,37], complex quantum oscillations controlled by the Aharonov-Casher phase, and weakly incoherent dynamics of quantum MF leading to the macroscopic Bloch oscillations [36] have been studied in detail. Moreover, the discrete sine-Gordon equation ceases to be an integrable one, and therefore, it is a good starting point to theoretically study the coherent quantum dynamics of high-order kinks trapped in JJAs.

In this paper a previously elaborated analysis of the quantum dynamics of a single MF [36] will be extended to the case of *two* MFs trapped in a JJPA with high kinetic inductances. The Josephson phase distribution of two MFs monotonically increases along the JJPA, and the total variation of Josephson phases is equal to 4π. In an almost anticontinuous limit each MF is characterized by Josephson phases of three consecutive Josephson junctions [36], and using this approximation we derive the repulsive interaction potential of two MFs and present the detailed study of the coherent quantum dynamics of two interacting MFs. In the analysis we distinguish two extreme dynamical patterns: the quantum dynamics of two independent MFs and a 4π kink, i.e., two merged MFs. For both cases we obtain the energy bands determining the coherent motion of two MFs along the JJPA, the time-dependent probability to find both MFs in a fixed cell of the JJPA, and macroscopic Bloch oscillations occurring in the presence of a weak dissipation. A quantitative comparison of these dynamic patterns allows one to obtain distinguished features of the 4π-kink coherent quantum dynamics.

The paper is organized as follows: In Sec. II we present our model for JJPAs with large kinetic inductances, and provide the generic expression for the potential energy $U(\{\varphi_i\})$, where $\{\varphi_i\}$ are the Josephson phases of individual Josephson junctions. In Sec. III we study the effective potential energy of two magnetic fluxons trapped in a JJPA. For that we use a special approximation where a single fluxon is characterized by Josephson phases of three consecutive Josephson junctions [36]. In Sec. IV we elaborate a two-dimensional tight-binding model allowing one to study the coherent quantum dynamics of two interacting magnetic fluxons. The quantum-mechanical dispersion relation of a 4π kink will be obtained. In Secs. V and VI we discuss the specific quantum properties of a 4π kink and compare that with two independent MFs. Section VII provides conclusions.

II. JJPAs WITH LARGE KINETIC INDUCTANCES: MODEL AND POTENTIAL ENERGY

Let us consider a JJPA composed of M small (quantum) Josephson junctions incorporated in superconducting cells of large kinetic inductances. The cell size is d. The dynamics of small Josephson junctions is determined by time-dependent Josephson phases, $\varphi_i(t)$, and these Josephson junctions can demonstrate the quantum-mechanical behavior on a macroscopic scale. Small Josephson junctions are characterized by two important physical parameters: the Josephson coupling energy, E_J, and the charging energy, E_c. Large kinetic inductances of superconducting cells are provided by series arrays of large (classical) Josephson junctions, δ_i. These series arrays of Josephson junctions allow one to effectively block the undesirable penetration of magnetic fluxes into JJAs. An external magnetic field piercing JJPA cells is characterized by the magnetic fluxes, Φ_i. The schematic of such setup is shown in Fig. 1(a).

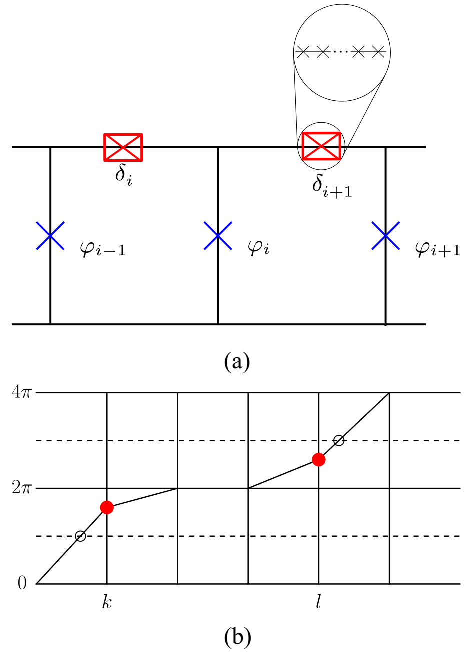

FIG. 1. (a) Schematic of a JJPA with large kinetic inductances. Small Josephson junctions with Josephson phases φ_i are shown by crosses. Large kinetic inductances are provided by series arrays of large Josephson junctions (shown by red boxes). (b) The typical Josephson phase distribution of two well separated MFs trapped in a JJPA. Red dots represent values of Josephson phases in the centers of the MFs and open circles represent "positions" of the MFs.

A general expression for the JJPA potential energy with the Josephson phase distribution $\{\varphi_i\}$ is given by

$$U(\{\varphi_i\}) = E_J \sum_{i=1}^{M} (1 - \cos\varphi_i) + E_L \sum_{i=1}^{M} \times \left(\varphi_i - \varphi_{i+1} + 2\pi \frac{(n_i\Phi_0 + \Phi_i)}{\Phi_0}\right)^2, \quad (1)$$

where n_i is number of magnetic flux quantum Φ_0 penetrating an ith cell. Here E_L is the kinetic inductance energy that is supposed to be small with respect to the Josephson coupling energy of individual Josephson junctions, E_J, i.e., $E_L \ll E_J$. Next we consider a simplest case as all Φ_i, n_i are set to zero.

III. JJPAs WITH TWO TRAPPED MAGNETIC FLUXONS

Next, we consider a particular case as two MFs are trapped in the JJPA. A single MF bearing the magnetic flux quantum Φ_0 is the 2π kink in the Josephson phase distribution $\{\varphi_i\}$, and correspondingly, in the presence of two MFs the $\{\varphi_i\}$ has to be a monotonic function and satisfy the following topological constraint: the total variation of φ_i along the JJPA is 4π.

To obtain the potential energy of two interacting MFs trapped in the JJPA with large kinetic inductances ($E_J \gg E_L$) we use the method elaborated previously to study the classical [38] and quantum [36] dynamics of a single MF in the anticontinuous limit, where a single MF is characterized by three consecutive Josephson phases, and other Josephson phases are set to 0 or 2π. To apply this method for the JJPA with two trapped MFs we fix the centers of MFs in cells k and ℓ. The Josephson phases of MF centers are φ_k varying in the region between 0 and 2π, and φ_l varying in the region between 2π and 4π, accordingly. The typical Josephson phase distribution of two well separated MFs is presented in Fig. 1(b).

A. Well separated MFs: $l-k \geqslant 3$

As the centers of MFs are located at large distances, e.g., $l-k=3$ [see the Josephson phase distribution in Fig. 1(b)], the Josephson phase distribution is written in the following form:

$$\{\varphi_i\} = \{0, \dots, 0, \varphi_{k-1}, \varphi_k, 2\pi + \tilde{\varphi}_{k+1}, 2\pi + \tilde{\varphi}_{l-1}, \\ 2\pi + \tilde{\varphi}_l, 4\pi - (2\pi - \tilde{\varphi}_{l+1}), 4\pi, \dots, 4\pi\}, \quad (2)$$

where we introduce the renormalized Josephson phase as $\tilde{\varphi}_n = \varphi_n - 2\pi$. Substituting (2) in (1) and taking into account that the Josephson phases φ_{k-1}, $|\tilde{\varphi}_{k+1}|$, $\tilde{\varphi}_{l-1}$, and $|\tilde{\varphi}_{l+1} - 2\pi|$ are small, we expand the potential energy (1) up to the second order with respect to these phases and minimize. Following this procedure and taking into account the terms up to the second order in E_L/E_J, we obtain the effective potential energy of two *noninteracting* MFs:

$$U_{\text{eff}}(\varphi_k, \tilde{\varphi}_{l=k+3}) = 2E_L\left(1 - \frac{2E_L}{E_J}\right)(\varphi_k^2 + \tilde{\varphi}_l^2) \\ - 4\pi E_L\left(1 - \frac{2E_L}{E_J}\right)(\varphi_k + \tilde{\varphi}_l) \\ + E_J(2 - \cos\varphi_k - \cos\tilde{\varphi}_l) + U_0, \quad (3)$$

where U_0 is obtained explicitly as

$$U_0 = 8E_L\pi^2 - 16\pi^2\frac{E_L^2}{E_J}. \quad (4)$$

Thus, one can see that the minimum of the effective potential energy occurs for small values of φ_k and $\tilde{\varphi}_l$, and the minimal value of (3) is $E_0 = U_0 - 16\pi^2 E_L^2/E_J$. Notice here that in the limit of $E_J \gg E_L$, Eq. (3) is valid also for MFs located at the distance $l-k \geqslant 3$.

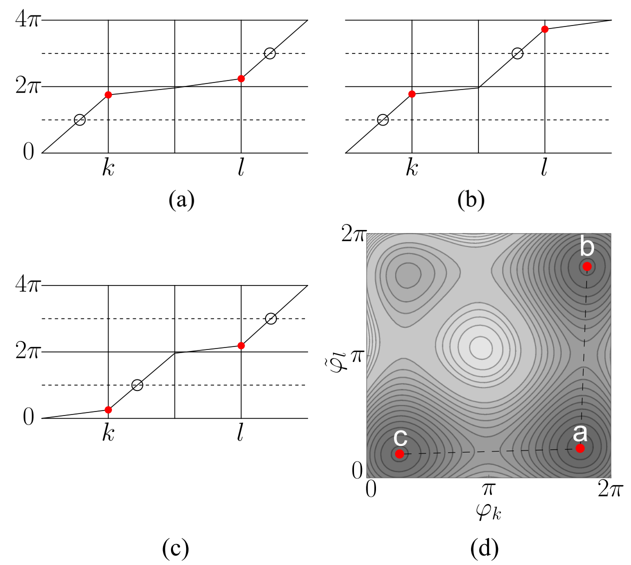

FIG. 2. The configurations of Josephson phases [(a), (b), and (c)] in the minima of $U_{\text{eff}}(l-k=2)$, and the contour plot (d) of the dependence of the effective potential energy on the Josephson phases, φ_k and $\tilde{\varphi}_l$, i.e., Eq. (6). The parameters were chosen as $E_J = 1$, $E_L = 0.1$.

B. Two MFs located at the distance $l-k=2$

Now we bring the MFs closer and the configuration of Josephson phases is

$$\{\varphi_i\} = \{0, \dots, 0, \varphi_{k-1}, \varphi_k, 2\pi + \tilde{\varphi}_{k+1}, \varphi_l, \\ 4\pi - (2\pi - \tilde{\varphi}_{l+1}), 4\pi, \dots, 4\pi\}. \quad (5)$$

By making use of the procedure analogous to the previous section we obtain the effective potential energy as

$$U_{\text{eff}}(\varphi_k, \tilde{\varphi}_{l=k+2}) = 2E_L\left(1 - \frac{2E_L}{E_J}\right)(\varphi_k^2 + \tilde{\varphi}_l^2) - 4\pi E_L \\ \times \left(1 - \frac{2E_L}{E_J}\right)(\varphi_k + \tilde{\varphi}_l) - \frac{4E_L^2}{E_J} \\ \times (2\pi - \varphi_k)\tilde{\varphi}_l + E_J(2 - \cos\varphi_k \\ - \cos\tilde{\varphi}_l) + U_0. \quad (6)$$

In the limit of $E_L \ll E_J$ the effective potential energy has three minima located near the points: $\{\varphi_k, \tilde{\varphi}_l\} = \{0, 0\}, \{2\pi, 0\}, \{2\pi, 2\pi\}$. Minimizing Eq. (6) over the Josephson phases φ_k and $\tilde{\varphi}_l$ we obtain explicit locations of the minima (we mark it with letters a, b, and c in Fig. 2) and the minimal energy, $U_{\min}$. The potential energy $U_{\min}$ at each minimum is the same up to the second order in E_L/E_J:

$$U_{\min}(|l-k| = 2) = 8E_L\pi^2 - 32\pi^2\frac{E_L^2}{E_J} = E_0. \quad (7)$$

Therefore, two MFs located at the distance $|l-k| = 2$ do not interact with each other. In Fig. 2 the configurations of the Josephson phases in minima of $U_{\text{eff}}(l-k=2)$ and the contour plot of the effective potential energy are presented.

In the quantum-mechanical regime the MFs can "hop" between the minima due to the macroscopic tunneling of the Josephson phases. Thus, the hopping amplitude is determined

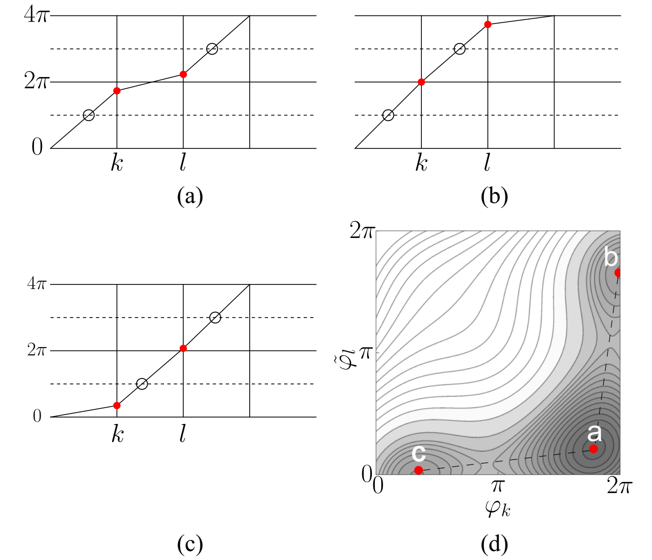

FIG. 3. The configurations of Josephson phases [(a), (b), and (c)] in the minima of $U_{\text{eff}}(l-k=1)$, and the contour plot (d) of the dependence of the effective potential energy on the Josephson phases, φ_k and $\tilde{\varphi}_l$, i.e., Eq. (10). The parameters were chosen as $E_J=1$, $E_L=0.1$.

by the potential energy profile between points a and b in the direction of $\varphi_k=\text{const}$ (see the dashed line in the contour plot of Fig. 2). We stress here that this profile is identical to the Josephson phase dependence of the potential energy of a single MF, i.e., the 2π kink, $U_{\text{eff}}^{2\pi}$, obtained in [36] as

$$U_{\text{eff}}^{2\pi}(\tilde{\varphi}_l)=2E_L\left(1-\frac{2E_L}{E_J}\right)\tilde{\varphi}_l^2-4\pi E_L\left(1-\frac{2E_L}{E_J}\right)\varphi_l + E_J(1-\cos\tilde{\varphi}_l)+\text{const}. \quad (8)$$

C. Two MFs located at the distance $l-k=1$

As the centers of two MFs are located in adjacent cells the Josephson phase configuration is written as

$$\{\varphi_i\}=\{0,\dots,0,\varphi_{k-1},\varphi_k,\varphi_l,4\pi-(2\pi-\tilde{\varphi}_{l+1}), 4\pi,\dots,4\pi\}. \quad (9)$$

Using the procedure elaborated in Secs. III A and III B we obtain the effective potential energy as

$$\begin{aligned}U_{\text{eff}}(\varphi_k,\tilde{\varphi}_{l=k+1}) &= 2E_L\left(1-\frac{2E_L}{E_J}\right)(\varphi_k^2+\tilde{\varphi}_l^2)-4\pi E_L\\ &\times\left(1-\frac{E_L}{E_J}\right)(\varphi_k+\tilde{\varphi}_l)+\frac{4E_L^2}{E_J}\pi(\tilde{\varphi}_l-\varphi_k)\\ &+2E_L(2\pi-\varphi_k)\tilde{\varphi}+E_J(2-\cos\varphi_k\\ &-\cos\tilde{\varphi}_l)+U_0-8\pi^2\frac{E_L^2}{E_J}.\end{aligned} \quad (10)$$

The expression (10) demonstrates the interaction between two MFs. Since $2\pi-\varphi_k\geqslant 0$ the interaction term is a positive one, and the MFs repel each other. The effective potential energy has three minima marked as a, b, and c in Fig. 3, and the values

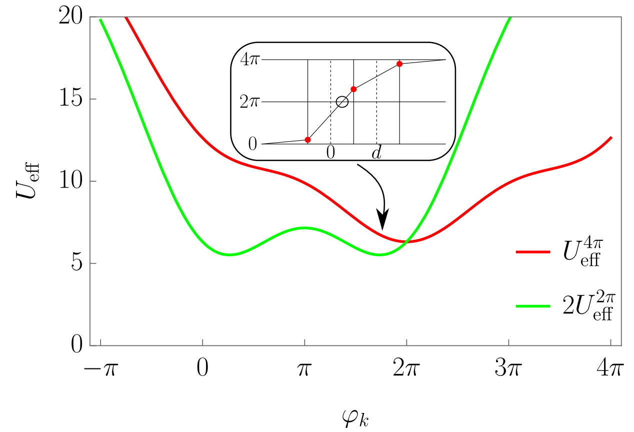

FIG. 4. Dependencies of the effective potential energies on the Josephson phase in the center of the 4π kink (red line) and two independent 2π kinks located on the same position (green line). The Josephson phase configuration of a stable 4π kink is shown in the inset. The parameters were chosen as $E_J=1$, $E_L=0.1$.

of $U_{\text{eff}}(l-k=1)$ in these minima are given by

$$\begin{aligned}U_{\min}(|l-k|=1)\Big|_a &\approx 8E_L\pi^2-32\pi^2\frac{E_L^2}{E_J}=E_0,\\ U_{\min}(|l-k|=1)\Big|_{b,c} &\approx 8E_L\pi^2-16\pi^2\frac{E_L^2}{E_J}=U_0=E_1.\end{aligned} \quad (11)$$

Here we denote the energy of higher minimum as E_1.

The tunneling amplitude from the state a to the state b is determined by the potential energy profile in the a-b direction that in the limit of $E_J\gg E_L$ is equal to $U_{\text{eff}}^{2\pi}(\varphi)$ [see Eq. (8)].

D. Two MFs located in the same cell: 4π kink

Here, we consider two MFs located in the same cell, i.e., 4π kink:

$$\{\varphi_i\}=\{0,\dots,0,\varphi_{k-1},\varphi_k,4\pi-(2\pi-\tilde{\varphi}_{k+1}),4\pi,\dots,4\pi\}. \quad (12)$$

For this Josephson phase configuration the potential energy is

$$U_{\text{eff}}^{4\pi}(\varphi_k)=2E_L\left(1-\frac{2E_L}{E_J}\right)\varphi_k^2-8\pi E_L\left(1-\frac{2E_L}{E_J}\right)\varphi_k + E_J(1-\cos\varphi_k)+2U_0. \quad (13)$$

The dependence of $U_{\text{eff}}^{4\pi}(\varphi_k)$ on the Josephson phase φ_k in the center of the 4π kink, is shown in Fig. 4. For comparison, the potential energy of two independent MFs located in the same cell, i.e., two 2π kinks, is also presented in Fig. 4.

The effective potential energy $U_{\text{eff}}^{4\pi}(\varphi_k)$ has a global minimum exactly at $\varphi_k=2\pi$ and its value at the minimum is $E_1=U_0$. As one can see, the 4π kink potential energy minimum is slightly higher than the potential energy of two independent MFs, and it coincides with the potential energy of two MFs in the configurations b, c presented in Fig. 3.

IV. ENERGY SPECTRUM OF TWO INTERACTING MFs: TIGHT-BINDING MODEL WITH INTERACTION

To quantitatively analyze the macroscopic quantum-mechanical phenomena we derive the energy spectrum of two interacting MFs. The kinetic energy of two MFs is expressed as $K\{\dot\varphi_k, \dot\varphi_l\} = E_J/(2\omega_p^2)[\dot\varphi_k^2 + \dot\varphi_l^2]$, where the plasma frequency $\omega_p = \sqrt{8E_J E_C}/\hbar$ was introduced. The effective Hamiltonian depending on two variables, φ_k and φ_l, is written as

$$\hat{H} = K\{\dot\varphi_k, \dot\varphi_l\} + U_{\rm eff}(\varphi_k, \varphi_l), \tag{14}$$

where the dependence of the potential energy $U_{\rm eff}$ on the distance $|l-k|$ between the cells k and l was obtained in Sec. III. As one can see from Figs. 2(d)–4(d) the centers of MFs are strongly localized in the minima of $U_{\rm eff}$, and in the quantum regime the MF tunneling between adjacent cells is just allowed. With these assumptions and using a standard procedure elaborated, e.g., in [39], the Hamiltonian (14) is reduced to the *tight-binding model* for two interacting quantum particles. In this model the wave function of two interacting MFs, $|\Psi\rangle$, is presented as the superposition of localized wave functions defined on the two-dimensional grid, i.e.,

$$|\Psi\rangle = \sum_{kl} c_{k,l}|k,l\rangle. \tag{15}$$

Here, the positive integers k and l, determining the coordinates of the grid's nodes, indicate the numbers of cells where the centers of MFs are located; $c_{k,l}$ are the quantum-mechanical amplitudes. Substituting (15) for (14) and taking into account the matrix elements $\langle k,l|\hat{H}|k,l\rangle$ and $\langle k\pm1,l|\hat{H}|k,l\rangle$ ($\langle k,l\pm1|\hat{H}|k,l\rangle$) only, we catch the tight-binding Hamiltonian of two interacting particles in the following form:

$$\begin{aligned}\hat{H} &= \sum_{kl} E_{kl}|k,l\rangle\langle k,l| - \frac{\Delta}{2}{\sum_{kl}}'(|k,l\rangle\langle k+1,l| \\ &\quad + \langle k,l\rangle\langle k,l+1| + \text{H.c.}), \\ E_{kl} &= E_0 + (E_1 - E_0)(\delta_{k,l} + \delta_{k,l+1} + \delta_{k,l-1}).\end{aligned} \tag{16}$$

Here, the matrix elements $\langle k,l|\hat{H}|k,l\rangle$ determine the localized state energies as E_0 if $|l-k|>1$ and E_1 for $l=k$ and $l=k\pm1$. The matrix elements $\langle k\pm1,l|\hat{H}|k,l\rangle$ ($\langle k,l\pm1|\hat{H}|k,l\rangle$) determine the amplitude of tunneling between the minima of the potential $U_{\rm eff}$ and provide the hopping amplitude Δ between the localized states on the adjacent grid's nodes. The explicit expression for the hopping amplitude $\Delta \simeq (\hbar\omega_p)\exp[-8E_J/(\hbar\omega_p)]$ has been obtained in [31,36,37]. Notice here, that the $\sum'$ indicates the absence of tunneling between the states with the energy E_1, i.e., between the grid's nodes $k=l$ and $l=k\pm1$.

The schematic of such tight-binding model is presented in Fig. 5. This procedure resembles the one elaborated previously for the analysis of two interacting quantum particles (e.g., bosons) moving on a one-dimensional periodic lattice [40,41].

For an explicit calculation of the energy spectrum of two interacting MFs it is convenient to align one of the coordinate axes in the $k=l$ direction and to use other integers $n=k-l$ and $m=k+l$ with the corresponding modification of the grids, $(k,l)\to(m,n)$. In this representation we rewrite the Hamiltonian as

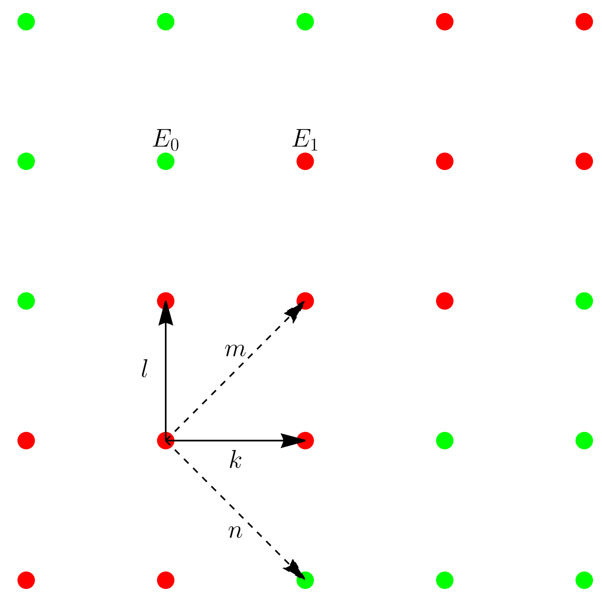

FIG. 5. The two-dimensional grid for the tight-binding model of two interacting quantum MFs. Such tight-binding model has a defect extended along the $k=l$, $l\pm1$ directions (indicated by red dots). Red dots have the higher energy E_1 and green dots have the lower energy E_0. Vectors $\vec{k}$, $\vec{l}$ and $\vec{m}=\vec{k}+\vec{l}$ and $\vec{n}=\vec{k}-\vec{l}$ are shown.

$$\begin{aligned}\hat{H} = &\sum_{\substack{kl \\ m=k+l \\ n=k-l}} E_{mn}|m,n\rangle\langle m,n| - \frac{\Delta}{2}{\sum_{\substack{kl \\ m=k+l \\ n=k-l}}}'(|m,n\rangle\langle m+1,n+1| \\ &+ |m,n\rangle\langle m+1,n-1| + \text{H.c.}), \\ E_{mn} = &E_0 + (E_1 - E_0)(\delta_{n,0} + \delta_{n,1} + \delta_{n,-1}),\end{aligned} \tag{17}$$

and the wave function has the following form: $|\psi\rangle = \sum_{k,l} c_{m,n}|m,n\rangle$. To obtain the energy spectrum E and wave functions ψ of two interacting quantum MFs, the stationary Schrödinger equation for amplitudes $c_{m,n}$ has to be written. The stationary Schrödinger equation presents a set of difference equations with the lattice defect extended along the $n=0,\pm1$ directions: the energy of cites $n=0,\pm1$ is $E_1 > E_0$. We treat cites with indices $n=-1,0,1$ as a single cite because they correspond to the same MFs configuration. Thus, the direct tunneling from the cites $n=-1,0,1$ to the cites $n=\pm2$ is allowed. The difference equations for coefficients $c_{m,n}$ on a whole grid are

$$\begin{aligned}&(E_0 - E)c_{m,n} - \frac{\Delta}{2}(c_{m+1,n+1} + c_{m+1,n-1} + c_{m-1,n+1} \\ &\quad + c_{m-1,n-1}) = 0,\ |n|>1; \\ &(E_1 - E)c_{m,1} - \frac{\Delta}{2}(c_{m+1,2} \\ &\quad + c_{m+1,-2} + c_{m-1,2} + c_{m-1,-2}) = 0; \\ &c_{m,-1} = c_{m,0} = c_{m,1}.\end{aligned} \tag{18}$$

A. Scattering states of two interacting quantum MFs

First, we describe the *scattering* states of two interacting MFs. Far away from the defect ($|n| > 1$) we search the solution $c_{m,n}$ for such states in the form of plane waves

$$c_{m,n} = \exp\left\{i\frac{p_1kd + p_2ld}{\hbar}\right\} = \exp\left\{i\frac{p(md/2) + qnd}{\hbar}\right\}, \tag{19}$$

where p_1 and p_2 are quasimomenta of first and second MFs. The $p = (p_1 + p_2)$ and $q = (p_1 - p_2)/2$ are the center of mass and relative quasimomenta of two MFs, accordingly.

Substituting this expression in the first equation of (18) we obtain the two-dimensional energy band spectrum $E(p, q)$ as

$$E_{2\times 2\pi}(p, q) = E_0 - 2\Delta \cos\left[\frac{pd}{2\hbar}\right] \cos\left[\frac{qd}{\hbar}\right]. \tag{20}$$

Thus, one can see that the quantum dynamics of two MFs with the energy spectrum (20) is determined by a weak scattering as the centers of two MFs approach each other at the distance of d. The energy band spectrum $E_{2\times 2\pi}(p, q)$ is just a sum of energies of independent MFs.

B. The bound states of two interacting MFs: 4π-kink quantum dynamics

In spite of the presence of a short range repulsive interaction between two MFs, the tight-binding Hamiltonian (17) supports also a one-dimensional band of bound states solutions. These states are strongly localized on grid nodes, $k = l$, and therefore correspond to the quantum 4π kinks. Since the energy spectrum of bound states is separated from the scattering states considered in Sec. IV A by the energy gap, the quantum dynamics of 4π kinks can be destroyed by interband relaxation processes only.

The quantitative analysis of the energy spectrum of quantum 4π kinks is provided as follows. The bound state amplitudes $c_{m,n}$ are caught in the form

$$c_{m,n} = e^{ipmd/(2\hbar)}[-\mathrm{sgn}(\eta)]^n e^{-|n|d/\lambda}, \tag{21}$$

where λ is the characteristic length of the bound state of two MFs, and $\eta = \cos[pd/(2\hbar)]$. Substituting (21) in the first equation of (18) we obtain the energy $E_{4\pi}$ as follows:

$$E_{4\pi} = E_0 + 2\Delta|\cos[pd/(2\hbar)]|\cosh(d/\lambda). \tag{22}$$

Substituting (22) in the second equation of (18) we obtain λ, and finally, the energy spectrum $E_{4\pi}(p)$ as

$$E_{4\pi}(p) = E_0 + \sqrt{4\Delta^2\cos^2[pd/(2\hbar)] + (E_1 - E_0)^2}. \tag{23}$$

Thus, one can see that the bound states of two MFs are characterized by a one-dimensional energy band spectrum, $E_{4\pi}(p)$, determining the quantum dynamics of a 4π kink trapped in the JJPA.

V. THE COHERENT QUANTUM OSCILLATIONS OF TWO INTERACTING MFs

In the previous section we obtain that the quantum dynamics of two MFs trapped in a one-dimensional JJPA can be realized in two forms: two weakly interacting moving MFs (the scattering states) or moving 4π kinks (the bound states). The coherent quantum dynamics of two MFs is determined by the probability $P(k, l; t)$ to find the MFs in cells k and l at the time t if initially both MFs were in cell 0. For the 4π kink we obtain

$$P_{4\pi}(k = l, t) = \left|d\int_{-\pi\hbar/d}^{\pi\hbar/d}\frac{dp}{2\pi\hbar}\exp\left\{-\frac{iE_{4\pi}(p)t}{\hbar} - \frac{ipkd}{\hbar}\right\}\right|^2. \tag{24}$$

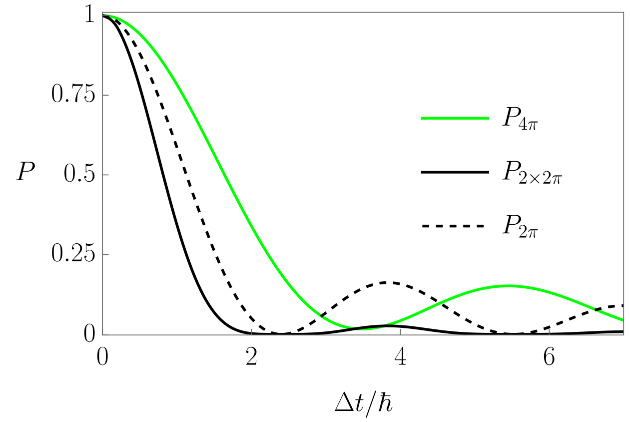

FIG. 6. Probabilities of finding 4π kink (green solid line), two independent fluxons (black solid line), and a single fluxon (black dashed line) in cell number 0 at time t. Here, we chose the parameter $\Delta/(E_0 - E_1) = 1/\sqrt{2}$.

Taking into account the energy band spectrum of a 4π kink, i.e., (23), one can calculate numerically $P_{4\pi}(k = l, t)$ for different values of Δ and $(E_1 - E_0)$. The typical time dependence of $P_{4\pi}(0, t) = P_{4\pi}(t)$, i.e., the *return* probability, is presented in Fig. 6. Moreover, in the limit of $(E_1 - E_0) \gg \Delta$ one can obtain an explicit expression $P_{4\pi}(t) = J_0^2[\frac{\Delta^2}{(E_1-E_0)\hbar}t]$, where $J_0(x)$ is the Bessel function [42]. Similarly, for scattering states of two weakly interacting MFs we obtain the $P_{2\times 2\pi}(k, l; t)$ as follows:

$$P_{2\times 2\pi}(k, l; t) = \left|d^2\iint\frac{dp\,dq}{(2\pi\hbar)^2}\exp\left\{-\frac{2i\Delta}{\hbar}t\cos\frac{pd}{2\hbar}\times\cos\frac{qd}{\hbar} - \frac{iq(k-l)d}{\hbar} - \frac{ip(k+l)d}{2\hbar}\right\}\right|^2. \tag{25}$$

The probability $P_{2\times 2\pi}(0, 0; t) = P_{2\times 2\pi}(t)$ is calculated explicitly as $P_{2\times 2\pi}(t) = J_0^4[\Delta t/\hbar]$ [42]. Both time dependencies of $P_{4\pi}(t)$ and $P_{2\times 2\pi}(t)$ are presented in Fig. 6. For comparison the time dependence of the return probability for a single MF, $P_{2\pi}(0, t) = P_{2\pi}(t) = J_0^2(\Delta t/\hbar)$, is also shown in Fig. 6.

To conclude this section we note that the applied gate voltage V_g provides the macroscopic Aharonov-Casher phase $\chi \propto V_g$ allowing one to vary the return probability $P_{4\pi}(t)$ in short annular JJPAs [36].

VI. WEAKLY DISSIPATIVE QUANTUM DYNAMICS OF A 4π KINK: BLOCH OSCILLATIONS AND CURRENT STEPS

In order to quantitatively characterize a weakly dissipative quantum dynamics of a 4π kink we introduce the coordinate ("position") $x_{4\pi}$ of the 4π kink in the JJPA as $x_{4\pi} = kd + d(4\pi - \varphi_k)/4\pi$, where φ_k is the Josephson phase in the center of the 4π kink located in the kth cell. The velocity operator $\dot{\hat{x}}$ is defined in a standard way as

$$\dot{\hat{x}}_{4\pi} = \frac{dE_{4\pi}(p)}{dp}, \tag{26}$$

where $E_{4\pi}(p)$ is the dispersion law of the 4π kink [see Eq. (23)]. Taking into account the Josephson relation $2eV = \hbar\dot{\varphi}$ one can obtain the voltage operator for the 4π kink as $2e\hat{V}_{4\pi} = 4\pi\hbar\dot{\hat{x}}_{4\pi}/d$.

An applied external current bias $I(t)$ results in an additional term in the effective Hamiltonian $[4\pi/(2ed)]I(t)\hat{x}$, and weakly dissipative effects are taken into account by tracing out the bath degrees of freedom [43–45]. We notice that this approach is suitable to describe the *intraband* dissipation arising from a weak interaction of MFs with a general type of environment, e.g., an external impedance circuit [45]. Moreover, such dissipation can be characterized by a single phenomenological parameter γ, i.e., the intraband inverse relaxation time.

Summarizing, we obtain the equation describing the 4π-kink dissipative quantum dynamics as follows:

$$\dot{p}_{4\pi} = \frac{4\pi\hbar}{2ed}I(t) - \gamma\mu\frac{dE_{4\pi}(p)}{dp}, \tag{27}$$

where $\mu = (4\pi)^2 E_J/(\omega_p d)^2$ is the effective mass.

Next, we consider the case of dc current bias $I(t) = I$ and obtain the I-V curve of a JJPA with a trapped 4π kink. Substituting (23) in (27) we rewrite the dynamic equation (27) as

$$\dot{p} = \frac{4\pi\hbar I}{2ed} + \frac{\gamma\mu d\Delta^2\sin(dp/\hbar)}{\hbar\sqrt{(E_0 - E_1)^2 + 4\Delta^2\cos^2(pd/(2\hbar))}}. \tag{28}$$

As the dc bias current I is smaller than the critical value I_t, the dynamic equation (28) supports a steady solution $\dot{p} = 0$ resulting in the linear part of the current-voltage characteristics, $V \propto I$. The expression for I_t is obtained explicitly as

$$I_t = I_0\sqrt{1 + \frac{\lambda^2}{2} + \lambda\sqrt{1 + \frac{\lambda^2}{4}}},$$
$$I_0 = \frac{ed^2\gamma\mu}{8\Delta\pi\hbar^2}, \tag{29}$$
$$\lambda = \frac{E_1 - E_0}{\Delta}.$$

For $I > I_t$ the quasimomentum $p(t)$ depends periodically on time resulting in the nonlinear part of the I-V curve. The numerical procedure to obtain the I-V curve is the following: we fix the dc bias I, solve Eq. (28) numerically, and calculate the time averaging of the voltage $\langle V_{4\pi}(t)\rangle$. After that we increase the dc bias current I and repeat the procedure. Obtained in this way, the I-V curves are presented in Fig. 7. Thus, one can see the Bloch nose type of the current-voltage characteristics also for the 4π-kink dynamics. The I-V curve of the 4π kink deviates substantially from the one obtained for two *independent* MFs. Indeed, for a fixed dc current bias the average voltage drop $\langle V_{2\times 2\pi}\rangle$ is just twice the voltage of a single MF. The current-voltage characteristics of a JJPA with two trapped independent MFs is shown in Fig. 7 by the dashed line.

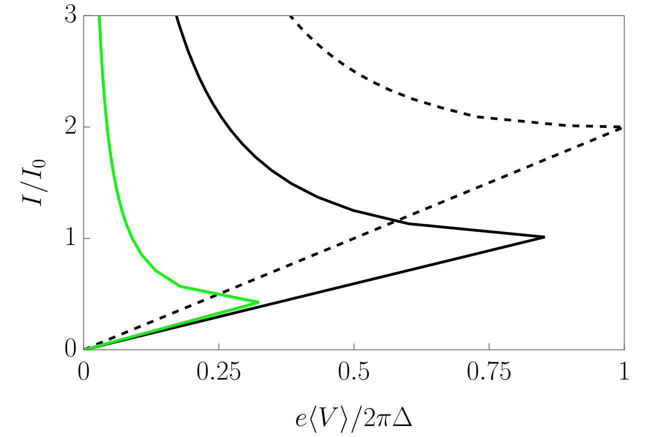

FIG. 7. The current-voltage characteristics of the JJPA with the trapped 4π kink. The parameters were chosen as $(E_1 - E_0)/\Delta = 0$ (black solid line) and $(E_1 - E_0)/\Delta = 3$ (green solid line). For comparison the I-V curve for two independent MFs trapped in a JJPA is shown by the dashed line.

For $I > I_t$ the voltage $V_{4\pi}(t)$ demonstrates large amplitude periodic oscillations, i.e., Bloch oscillations. In the limit of $I \gg I_t$ the frequency of 4π kink Bloch oscillations is $f^{Bl}_{4\pi} = I/e$. In the presence of both dc current I and ac current with the frequency f, the resonance between the Bloch oscillations and an external ac current leads to the seminal current steps [44,46] located at $I^{(n)}_{4\pi} = enf$. It is important to stress here that the current step values $I^{(n)}_{4\pi}$ for the 4π kink are two times less than those for two independent MFs, i.e., $I^{(n)}_{4\pi} = (1/2)I^{(n)}_{2\times 2\pi}$.

To conclude this section we note that the negative differential resistance (see Fig. 7) obtained in a weakly dissipative quantum dynamics of MFs trapped in JJPAs can be used to realize a stable source of microwave radiation similarly to the one based on the Josephson vortex dynamics in layered high-T_c materials [47–49].

VII. CONCLUSION

In conclusion we present a detailed theoretical study of the quantum dynamics of two magnetic fluxons trapped in a JJPA with large kinetic inductances. In such JJPAs the characteristic size of a single MF is less than the cell size, and a discrete sine-Gordon model close to the anticontinuous limit adequately describes the dynamics of trapped MFs. Characterizing the Josephson phase distribution of a single MF by three consecutive Josephson phases, we derive the effective potential energy of two interacting MFs, and obtain that the two MFs repel each other as they occupy the same or neighboring cells. Unexpectedly, in spite of the presence of a repulsive local interaction between two MFs, the quantum dynamics of two merged MFs, i.e., a 4π kink, can be realized in such JJPAs.

The quantum dynamics of a 4π kink in a JJPA is determined by the energy band spectrum $E_{4\pi}(p)$ [see Eq. (23)]. In the coherent quantum regime such spectrum leads to the quantum beats of the time-dependent return probability to observe the 4π kink on the initial point after time t. The amplitude and frequency of these quantum beats differ substantially from those observed for two independently propagating MFs.

In the presence of a weak *intraband* dissipation the periodic dependence of the energy spectrum $E_{4\pi}(p)$ on the quasimomentum p results in the 4π-kink Bloch oscillations with the frequency $f_{4\pi}^{\rm Bl}$ determined by an applied dc bias current, I, and the nonlinear current-voltage characteristics with the typical "Bloch nose." The resonance between the intrinsic Bloch oscillations and an externally applied ac current provides current steps with values $I_{4\pi}^{(n)} = enf$ that are two times less than those for two independent MFs. Notice here that an overall stability of 4π-kink quantum dynamics is determined by the interband relaxation processes.

A possibility of experimental observations of the quantum dynamics of interacting MFs crucially depends on a lifetime of MFs trapped in JJPAs. A most important process leading to the escape of MFs out of the array through its boundaries is the phase slips. A great advantage of JJPAs with high kinetic inductances is that the lifetime of trapped MFs drastically increases. Indeed, as a high kinetic inductance is achieved by the addition of a series of N Josephson junctions with Josephson energy $E_{J0} \gg E_J$ and charging energy $E_{c0} \ll E_c$ in the cells of the array (see red boxes in Fig. 1), the MF's lifetime can be estimated as $\tau \simeq (\omega_{p0})^{-1} N \exp[-\alpha\sqrt{E_{J0}/E_{c0}}]$ (the parameter α is the numerical coefficient of order one). On other hand, the inductive energy $E_L = E_{J0}/N$ has to be smaller than E_J. Thus by choosing large $N \sim 100$ and $E_{J0} \sim 10E_J$ one can satisfy both conditions of high kinetic inductance and large lifetime of MFs.

Finally, we would like to stress that our analysis of the quantum dynamics of interacting MFs is based on the generic discrete sine-Gordon model close to the anticontinuous limit, and therefore, our results can be applicable to other solid-state systems, e.g., low-dimensional antiferromagnets [29].

ACKNOWLEDGMENTS

We thank Sergej Mukhin and Alexey Ustinov for fruitful discussions. This work was partially supported by the Ministry of Science and Higher Education of the Russian Federation in the framework of the State Program (Project No. 0718-2020-0025).

[1] N. Manton and P. Sutcliffe, *Topological Solitons* (Cambridge University Press, Cambridge, UK, 2004).

[2] Y. V. Kartashov, B. A. Malomed, and L. Torner, Solitons in nonlinear lattices, Rev. Mod. Phys. **83**, 247 (2011).

[3] A. Scott, *Nonlinear Science* (Oxford University Press, Oxford, 1999), Vol. 4.

[4] O. M. Braun, Y. Kivshar, and Y. S. Kivshar, *The Frenkel-Kontorova Model: Concepts, Methods, and Applications* (Springer Science & Business Media, Berlin, 2004).

[5] Y. S. Kivshar and B. A. Malomed, Dynamics of solitons in nearly integrable systems, Rev. Mod. Phys. **61**, 763 (1989).

[6] A. Ustinov, Solitons in Josephson junctions, Phys. D (Amsterdam, Neth.) **123**, 315 (1998).

[7] J. J. Mazo and A. V. Ustinov, The sine-Gordon equation in Josephson-junction arrays, in *The Sine-Gordon Model and its Applications* (Springer, New York, 2014), pp. 155–175.

[8] G. Carapella, G. Costabile, and R. Latempa, Coherent fluxon motion in parallel arrays of long Josephson junctions, Philos. Mag. B **80**, 857 (2000).

[9] I. Vernik, N. Lazarides, M. Sørensen, A. Ustinov, N. F. Pedersen, and V. Oboznov, Soliton bunching in annular Josephson junctions, J. Appl. Phys. **79**, 7854 (1996).

[10] A. Wallraff, A. V. Ustinov, V. V. Kurin, I. A. Shereshevsky, and N. K. Vdovicheva, Whispering Vortices, Phys. Rev. Lett. **84**, 151 (2000).

[11] M. V. Fistul and A. V. Ustinov, Libration states of a nonlinear oscillator: Resonant escape of a pinned magnetic fluxon, Phys. Rev. B **63**, 024508 (2000).

[12] A. V. Ustinov, C. Coqui, A. Kemp, Y. Zolotaryuk, and M. Salerno, Ratchetlike Dynamics of Fluxons in Annular Josephson Junctions Driven by Biharmonic Microwave Fields, Phys. Rev. Lett. **93**, 087001 (2004).

[13] P. Binder, D. Abraimov, A. V. Ustinov, S. Flach, and Y. Zolotaryuk, Observation of Breathers in Josephson Ladders, Phys. Rev. Lett. **84**, 745 (2000).

[14] E. Trías, J. J. Mazo, and T. P. Orlando, Discrete Breathers in Nonlinear Lattices: Experimental Detection in a Josephson Array, Phys. Rev. Lett. **84**, 741 (2000).

[15] M. Peyrard and M. D. Kruskal, Kink dynamics in the highly discrete sine-Gordon system, Phys. D (Amsterdam, Neth.) **14**, 88 (1984).

[16] A. Champneys and Y. S. Kivshar, Origin of multikinks in dispersive nonlinear systems, Phys. Rev. E **61**, 2551 (2000).

[17] A. V. Ustinov, B. A. Malomed, and S. Sakai, Bunched fluxon states in one-dimensional Josephson-junction arrays, Phys. Rev. B **57**, 11691 (1998).

[18] J. Pfeiffer, M. Schuster, A. A. Abdumalikov, Jr., and A. V. Ustinov, Observation of Soliton Fusion in a Josephson Array, Phys. Rev. Lett. **96**, 034103 (2006).

[19] R. Fazio and H. Van Der Zant, Quantum phase transitions and vortex dynamics in superconducting networks, Phys. Rep. **355**, 235 (2001).

[20] H. S. J. van der Zant, W. J. Elion, L. J. Geerligs, and J. E. Mooij, Quantum phase transitions in two dimensions: Experiments in Josephson-junction arrays, Phys. Rev. B **54**, 10081 (1996).

[21] T. Kato and M. Imada, Macroscopic quantum tunneling of a fluxon in a long Josephson junction, J. Phys. Soc. Jpn. **65**, 2963 (1996).

[22] Z. Hermon, A. Stern, and E. Ben-Jacob, Quantum dynamics of a fluxon in a long circular Josephson junction, Phys. Rev. B **49**, 9757 (1994).

[23] A. Shnirman, E. Ben-Jacob, and B. Malomed, Tunneling and resonant tunneling of fluxons in a long Josephson junction, Phys. Rev. B **56**, 14677 (1997).

[24] A. Wallraff, Y. Koval, M. Levitchev, M. Fistul, and A. Ustinov, Annular long Josephson junctions in a magnetic field: Engineering and probing the fluxon interaction potential, J. Low Temp. Phys. **118**, 543 (2000).
[25] A. Wallraff, A. Lukashenko, J. Lisenfeld, A. Kemp, M. Fistul, Y. Koval, and A. Ustinov, Quantum dynamics of a single vortex, Nature (London) **425**, 155 (2003).
[26] M. V. Fistul, A. Wallraff, Y. Koval, A. Lukashenko, B. A. Malomed, and A. V. Ustinov, Quantum Dissociation of a Vortex-Antivortex Pair in a Long Josephson Junction, Phys. Rev. Lett. **91**, 257004 (2003).
[27] S. Coleman, Quantum sine-Gordon equation as the massive Thirring model, Phys. Rev. D **11**, 2088 (1975).
[28] D. N. Aristov and A. Luther, Correlations in the sine-Gordon model with finite soliton density, Phys. Rev. B **65**, 165412 (2002).
[29] M. Oshikawa and I. Affleck, Field-Induced Gap in $S = 1/2$ Antiferromagnetic Chains, Phys. Rev. Lett. **79**, 2883 (1997).
[30] V. E. Manucharyan, J. Koch, L. I. Glazman, and M. H. Devoret, Fluxonium: Single Cooper-pair circuit free of charge offsets, Science **326**, 113 (2009).
[31] I. N. Moskalenko, I. S. Besedin, S. S. Seidov, M. V. Fistul, and A. V. Ustinov, Quantum beats of a magnetic fluxon in a two-cell SQUID, Phys. Rev. B **103**, 224528 (2021).
[32] N. Maleeva, L. Grünhaupt, T. Klein, F. Levy-Bertrand, O. Dupre, M. Calvo, F. Valenti, P. Winkel, F. Friedrich, W. Wernsdorfer *et al.*, Circuit quantum electrodynamics of granular aluminum resonators, Nat. Commun. **9**, 3889 (2018).
[33] T. M. Hazard, A. Gyenis, A. Di Paolo, A. T. Asfaw, S. A. Lyon, A. Blais, and A. A. Houck, Nanowire Superinductance Fluxonium Qubit, Phys. Rev. Lett. **122**, 010504 (2019).
[34] O. Astafiev, L. Ioffe, S. Kafanov, Y. A. Pashkin, K. Y. Arutyunov, D. Shahar, O. Cohen, and J. S. Tsai, Coherent quantum phase slip, Nature (London) **484**, 355 (2012).
[35] M. Wildermuth, L. Powalla, J. N. Voss, Y. Schön, A. Schneider, M. V. Fistul, H. Rotzinger, and A. V. Ustinov, Fluxons in high-impedance long Josephson junctions, Appl. Phys. Lett. **120**, 112601 (2022).
[36] S. S. Seidov and M. V. Fistul, Quantum dynamics of a single fluxon in Josephson-junction parallel arrays with large kinetic inductances, Phys. Rev. A **103**, 062410 (2021).
[37] A. Petrescu, H. E. Türeci, A. V. Ustinov, and I. M. Pop, Fluxon-based quantum simulation in circuit QED, Phys. Rev. B **98**, 174505 (2018).
[38] B. Joos, Properties of solitons in the Frenkel-Kontorova model, Solid State Commun. **42**, 709 (1982).
[39] A. Altland and B. Simons, Interaction effects in the tight-binding system, in *Condensed Matter Field Theory* (Cambridge University Press, Cambridge, 2010), p. 59.
[40] M. V. Ivanchenko, T. V. Laptyeva, and S. Flach, Quantum chaotic subdiffusion in random potentials, Phys. Rev. B **89**, 060301(R) (2014).
[41] I. I. Yusipov, T. V. Laptyeva, A. Y. Pirova, I. B. Meyerov, S. Flach, and M. V. Ivanchenko, Quantum subdiffusion with two-and three-body interactions, Eur. Phys. J. B **90**, 66 (2017).
[42] M. Abramowitz and I. A. Stegun, *Handbook of Mathematical Functions with Formulas, Graphs, and Mathematical Tables*, 9th Dover printing, 10th GPO printing (Dover, New York, 1964).
[43] T. Dittrich, P. Hänggi, G.-L. Ingold, B. Kramer, G. Schön, and W. Zwerger, *Quantum Transport and Dissipation* (Wiley-VCH, Weinheim, 1998), Vol. 3.
[44] K. Likharev and A. Zorin, Theory of the Bloch-wave oscillations in small Josephson junctions, J. Low Temp. Phys. **59**, 347 (1985).
[45] G.-L. Ingold and Y. V. Nazarov, Charge tunneling rates in ultrasmall junctions, in *Single Charge Tunneling* (Springer, New York, 1992), pp. 21–107.
[46] G. Schön and A. D. Zaikin, Quantum coherent effects, phase transitions, and the dissipative dynamics of ultra small tunnel junctions, Phys. Rep. **198**, 237 (1990).
[47] N. F. Pedersen, G. Filatrella, V. Pierro, and M. P. Sørensen, Negative differential resistance in Josephson junctions coupled to a cavity, Phys. C (Amsterdam, Neth.) **503**, 178 (2014).
[48] S.-Z. Lin and A. E. Koshelev, Linewidth of the electromagnetic radiation from Josephson junctions near cavity resonances, Phys. Rev. B **87**, 214511 (2013).
[49] M. Tsujimoto, K. Yamaki, K. Deguchi, T. Yamamoto, T. Kashiwagi, H. Minami, M. Tachiki, K. Kadowaki, and R. A. Klemm, Geometrical Resonance Conditions for THz Radiation from the Intrinsic Josephson Junctions in $Bi_2Sr_2CaCu_2O_{8+\delta}$, Phys. Rev. Lett. **105**, 037005 (2010).